Thermally Induced Dynamics of Dislocations in Graphene at Atomic Resolution

Chuncheng Gong,[†] Alex W. Robertson,[†] Kuang He,[†] Gun-Do Lee,[‡] Euijoon Yoon,[‡] Christopher S. Allen,[†] Angus I. Kirkland,[†] and Jamie H. Warner*[,†]

[†]Department of Materials, University of Oxford, Parks Road, Oxford OX1 3PH, United Kingdom and [‡]Department of Materials Science and Engineering, Seoul National University, Seoul 151-742, Korea

ABSTRACT

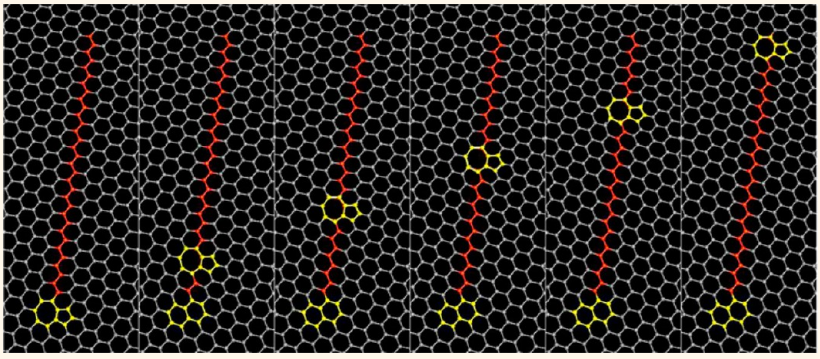

Thermally induced dislocation movements are important in understanding the effects of high temperature annealing on modifying the crystal structure. We use an *in situ* heating holder in an aberration corrected transmission electron microscopy to study the movement of dislocations in suspended monolayer graphene up to 800 °C. Control of temperature enables the differentiation of electron beam induced effects and thermally driven processes. At room temperature, the dynamics of dislocation behavior is driven by the electron beam irradiation at 80 kV; however at higher temperatures, increased movement of the dislocation is observed and provides evidence for the influence of thermal energy to the system. An analysis of the dislocation movement shows both climb and glide processes, including new complex pathways for migration and large nanoscale rapid jumps between fixed positions in the lattice. The improved understanding of the high temperature dislocation movement provides insights into annealing processes in graphene and the behavior of defects with increased heat.

KEYWORDS: TEM · graphene · dislocations · defects · 2D · aberration-corrected

The exceptional electronic, magnetic, and mechanical properties of graphene can be modulated by introducing defects and adatoms.[1−9] Dislocations have higher stability against quenching compared with other intrinsic defects such as monovacancies and divacancies.[10,11] A dislocation in graphene can be annihilated through either the recombination of two opposite orientated dislocations or by gliding toward the edge of graphene. The movement of dislocations plays a crucial role in determining the macroscopic plastic deformation of materials, especially at elevated temperatures. Thus, understanding the atomic structure and dynamics of dislocations in graphene is of significant importance for developing a complete structure model. Various work over the years has revealed that the motion of dislocations in CNT and graphene is quite different from that in three-dimensional crystals.[10,12−17] The migration of dislocations in graphene normally occurs by Stone−Wales (SW) bond rotations (glide) or the loss of a carbon dimer (climb) at certain positions. Due to the high surface-to-volume ratio, dislocations are also found to introduce rippling (out-of-plane distortion) in free suspended graphene.[18−22] Despite the large amount of research in the structural study of graphene, only few reports have focused

* Address correspondence to Jamie.warner@materials.ox.ac.uk;.

Received for review June 15, 2015 and accepted October 8, 2015.

Published online October 13, 2015
10.1021/acsnano.5b05355

© 2015 American Chemical Society

on the high temperature dynamics of defects and dislocations in graphene and other carbon nanomaterials. Kotakoski *et al.* studied the random walk and structural changes of divacancies in graphene under electron irradiation in an aberration-corrected scanning transmission electron microscope (STEM).[23] Suenaga *et al.* reported the direct imaging of pentagon-heptagon defects in a SWNT at equivalent temperatures of 2273 K, which are suggested to be responsible for the plasticity of the material.[24] He *et al.* studied the atomic structure of graphene edges at different temperatures using both TEM and STEM and proved the edge configuration in graphene is temperature dependent.[25] Huang *et al.* also performed *in situ* HR-TEM experiments at more than 2000 °C and observed the superplasticity of SWNTs and the shrinkage of giant fullerenes.[26,27] The dynamics for the migration of isolated dislocations at elevated temperatures has not yet been explored.

Aberration corrected transmission electron microscopy (AC-TEM) has been a powerful tool in resolving the graphene lattice and controllably creating defects in graphene with a focused beam. With aberration correction and a monochromated electron source, it is possible to obtain a spatial resolution of 80 pm.[16,28−32] Experimental analysis suggests that operating TEM at or below an accelerating voltage of 80 kV could remarkably reduce electron irradiation damage to the graphene specimen, but does not prevent occasionally sputtering of carbon atoms and bond rotations.[33−37]

In this report, we utilize an *in situ* heating holder within an AC-TEM to study the atomic structure and dynamics of dislocations in graphene at different temperatures. Defects were initially created by focusing the electron beam onto the sample using a previously reported approach and then searching for isolated dislocation cores to study.[30] An accelerating voltage of 80 kV is used to acquire atomic-resolution images with minimized knock-on damage when using a beam current density of $\sim 10^7$ e s^{-1} nm^{-2}. The contribution of electron beam impacts to the dynamics of dislocations may not depend heavily on temperature, and by increasing the temperature, we aim to see addition movement of dislocations that is associated with increasing thermal energy.

RESULTS AND DISCUSSION

The pentagon−heptagon (5−7) configuration is the most commonly reported structure of a dislocation core in graphene. The migration of a dislocation can be accomplished by either a Stone−Wales bond rotation (a glide step) or the removal of a carbon dimer (a climb step). The bond-rotation driven dislocation glide was reported by Yakobson as early as 1998 in simulating the mechanical relaxation in CNTs.[12] In 2007, Ding *et al.* further showed that the pseudoclimb of dislocation also plays a role in the plastic elongation of CNTs.[13,14] The activation energy for a bond rotation is calculated to be 5−10 eV, depending on the local sp^2-bond configurations.[38,39] Our density functional theory (DFT) calculation gives a value of 6.95 eV for a basic glide motion, which is significantly higher than the thermal vibration of the graphene lattice (0.068 eV, Figure S1), and results in a dislocation at room temperature that is fixed in its position. Figure 1 is an example showing a dislocation that remains in its position over 7 min and 13 s. However, in some cases under 80 kV electron irradiation, a SW rotation is induced by the electron beam, as is shown in Figure 1b,d.[40,41] Both rotated defects remain stable for more than 60 s, as the energy barrier for the SW rotation to unwind is ~5 eV.

Figure 2 shows a sequence of AC-TEM images of a dislocation core in graphene at 500 °C. The dislocation no longer stays immobile as it did at room temperature. It slowly shift its position by SW rotations, the trajectory of which is shown in Figure 2c. The migration path of the dislocation is one-dimensional restricted in the gliding plane at 500 °C. Four glide steps in a time period of about 9 min occurred. No climb steps were observed at room temperature or 500 °C. However, in Figure S2, we observed a complex migration equivalent to one basic glide plus climb steps over 133 s at 500 °C.

When the temperature of the specimen is increased to 700 °C, dislocations start to move more rapidly *via* both bond rotations and removal of carbon dimers. The migration path of a dislocation at 700 °C in 13 min and 38 s is shown in Figure 3. The time interval between each AC-TEM frame is ~13−15 s. Only the frames in which the dislocation shifts its position and is relaxed to the form of isolated pentagon−heptagon are included in Figure 3 (Figure 3n is an exception for the dislocation directly glided to its position in Figure 3o without the bond rotation reverted). Twenty-four glide and eight climb steps are detected during the imaging period. Another similar example is shown in Figure S3.

The trajectory of the dislocation in Figure 3 is apparently different from the previously reported random walk of point defects in graphene.[23] This is due to the different mechanisms for the glide and climb behavior. The glide motion for the 5−7 dislocation occurs rigorously along the Burger vector *via* the rotation of a carbon dimer by 90° of its middle point (marked by the red ellipse in Figure 4a). Since there is no other defect nearby for the dislocations in Figures 2 and 3 to interact with (Figure S4), it is of equal probability for the dislocation to glide toward both directions in the slip plane. On the other hand, the climb motion is perpendicular to the slip plane, requiring the removal of a pair of carbon atoms (highlighted by the green ellipse in Figure 4a). Theoretically, a dislocation can climb toward the opposite direction

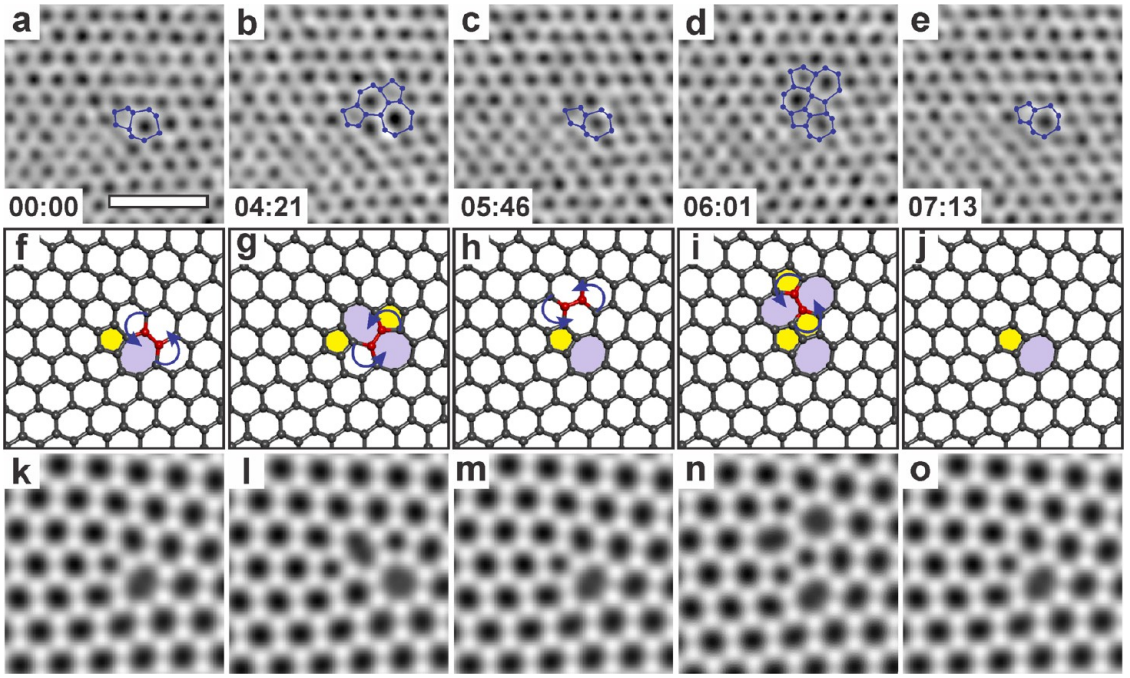

Figure 1. Beam-driven structural changes of a dislocation in graphene at room temperature. A total of 35 images were taken over 7 min and 13 s. (a−e) AC-TEM images showing the structural changes of a dislocation under electron irradiation. The lifetime of the structure shown in panels b and d is 73 ± 14 and 92 ± 14 s, respectively. (f−j) Atomic models of (a−e) with blue arrows and atoms highlighted in red indicating bonds that undergo a SW rotation in the next panel. The color scheme in the atomic models represents the number of carbon atoms in each ring, with 5 = yellow and 7 = blue. (k−o) Multislice simulated TEM images using the atomic models in (f−j), respectively. The scale bar in panel a is 1 nm.

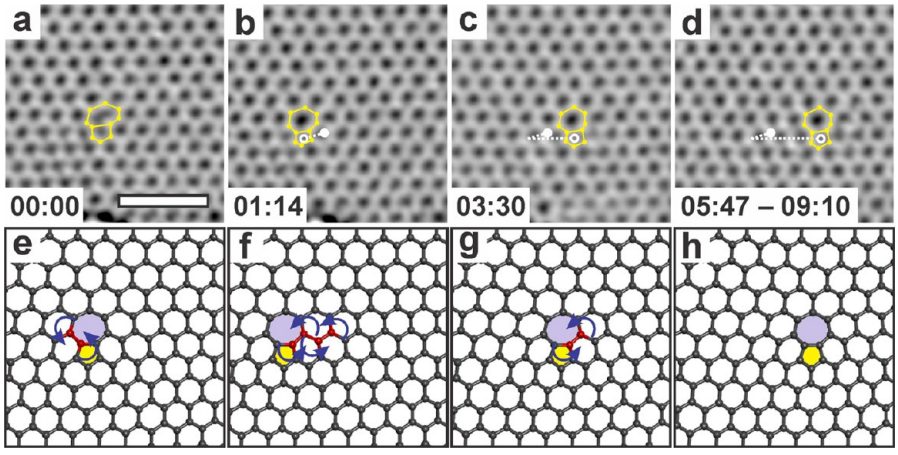

Figure 2. Migration path for a dislocation in graphene at 500 °C. A total of 39 frames were taken over a period of about 9 min and 10 s. (a−d) ACTEM images showing the position of an isolated dislocation core. The trajectory is drawn by connecting the central point of the pentagon from each dislocation with white dashed lines. The start and end position are indicated by a filled and a hollow circle, respectively. (e−h) Corresponding atomic models. The scale bar in panel a is 1 nm.

by introducing two extra carbon atoms to the graphene lattice, which is however not observed in this specific study. This is probably because after the ejection of the first carbon atom, it requires far less energy to sputter the under-coordinated carbon atom, while successively incorporating two carbon atoms into the graphene lattice is a more difficult process. Thus, all the climb components in the trajectory are in the same direction, which leads to the migration path schematically shown in Figure 4b with glide motions combined.

We now discuss the theory for the dependence of both glide and climb steps on temperature. The behavior for dislocation glide can be explained by the two-dimensional diffusion. According to the definition of two-dimensional diffusivity, the diffusion coefficient is calculated by

$$D = \frac{\bar{\delta}^2}{4\tau}$$

where $\bar{\delta}$ is the average jump distance and τ the jump time. We assume that the glide motion over more than

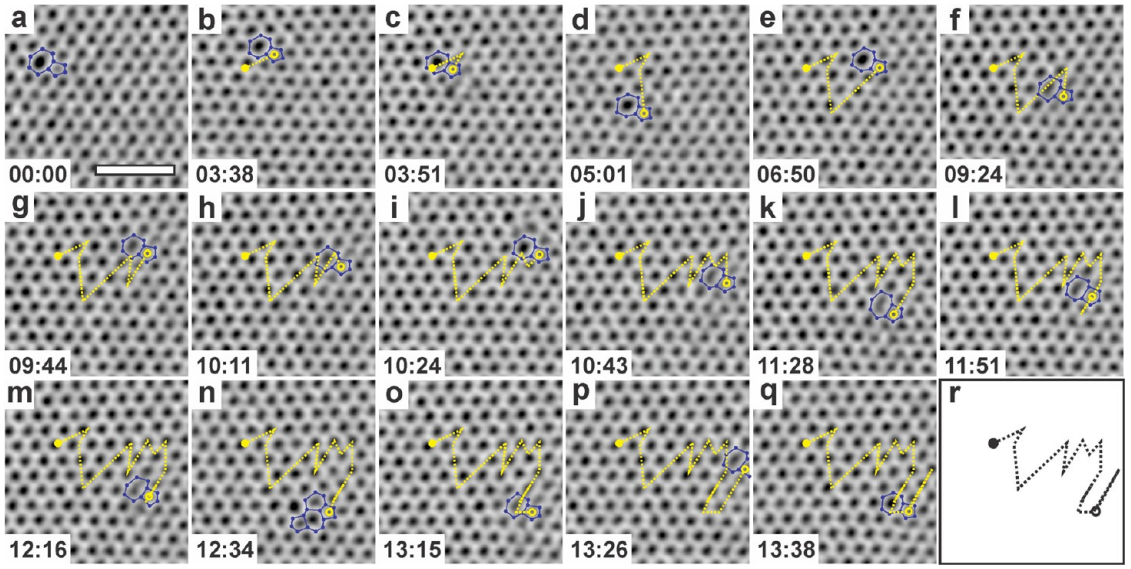

Figure 3. Trajectory of a dislocation in graphene at 700 °C. A total of 63 frames were recorded over 14 min and 30 s. Only those frames where the dislocation is in the form of an isolated pentagon−heptagon (expect panel n) are included. The scale bar in panel a is 1 nm.

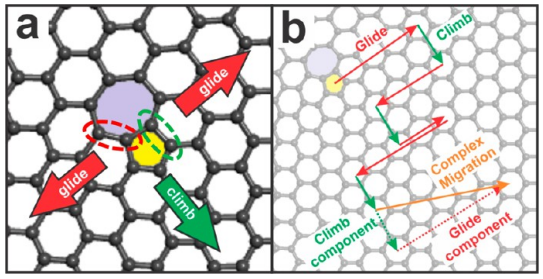

Figure 4. Schematic diagrams showing the possible migration directions for dislocations in graphene. (a) A dislocation can migrate along the gliding plane *via* bond rotations (basic glide step, indicated by the red arrows) or perpendicularly to the gliding plane *via* the removal of a carbon dime (basic climb step, marked by the green arrow). (b) Schematic trajectory of a dislocation with both glide and climb motions involved. A complex migration step can be regarded as several equivalent basic glide and climb steps, which is particularly discussed in Figures 6−10

one lattice is accomplished by several separate basic steps. The jump distance of each step is approximately equivalent to the graphene lattice constant 0.24 nm. Some migration steps consist of both glide and climb behavior and only the displacement in gliding plane is taken into calculation. By analyzing the data in Figures 2 and 3, we get $D \approx 1.51 \times 10^{-4}$ nm^2 s^{-1} (773 K) and 4.10×10^{-4} nm^2 s^{-1} (973 K). In our experiment, the glide motion of the dislocation is driven by both the thermal energy and electron beam irradiation. The relation between diffusion coefficient and experimental conditions is given by

$$D = D_0 \exp\left(-\frac{E_b}{k_b T + E_{beam}}\right)$$

in which D_0 is the diffusion constant, $k_b = 8.617 \times 10^{-5}$ eV/K is the Boltzmann constant, and E_b is the diffusion energy barrier for a bond rotation which is 6.95 eV calculated by our DFT method. E_{beam} represents the contribution of electron beam in driving dislocation glide, while k_bT represents the contribution from thermal energy. The distribution of calculated number of scattering events with transferred energy is shown in Figure S5, which is in proportion to the beam current density. Since the imaging condition (beam current density) is basically the same for experiments at different temperatures, E_{beam} should be a constant. By putting our experimental measured diffusion coefficient into the equation, we get

$$\frac{D_1}{D_2} = \exp\left(-\frac{E_b}{k_b T_1 + E_{beam}} + \frac{E_b}{k_b T_2 + E_{beam}}\right)$$

E_{beam} is the only unknown in the expression, and solving gives $E_{beam} \approx 0.353$ eV.

The theory above can only be used to analyze the temperature-dependent glide motions. The climb behavior, however, needs to overcome a much higher energy barrier and further involves atom loss. It is studied by calculating the sputtering cross section using the analytical method developed by Meyer *et al.*[36] The minimum energy to sputter a three-coordinated carbon atom from the pristine graphene lattice is approximately 22 eV.[33,36,42,43] However, a dislocation introduces an out-of-plane distortion in the local area. The displacement threshold energies in curved area are calculated to be lower.[14] The threshold for removing a carbon atom from the pentagon in a 5−7 configured dislocation is calculated to be 2−3 eV lower.[17] Thus, we assume the threshold for a climb process is 19 eV and calculated the sputtering cross section as a function of temperature, the result of which is shown in Figure 5 and Table 1. The cross section for sputtering a carbon atom in the pentagon is

40−600 times that in the perfect lattice, which explains why we only observe atom loss in or next to the dislocation rather than the creation of new defects in the pristine lattice. The curve shows a strong positive correlation between the sputtering cross section with a 19 eV-threshold and specimen temperature, which provide theoretical support for the temperature-dependency of the climb motion.

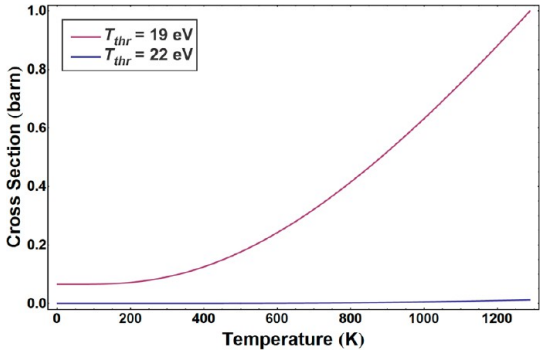

Figure 5. Dependence of carbon displacement cross section on temperature where sputtering threshold energy is 22 eV (blue) and 19 eV (red).

TABLE 1. Comparison of Displacement Cross Sections at Three Different Temperatures Where Thresholds Are 19 and 22 eV, Respectively

		temperature (K)		
		293	773	973
sputtering cross section (barn)	T_{thr} = 19 eV	0.0893	0.390	0.602
	T_{thr} = 22 eV	1.43×10^{-4}	5.84×10^{-3}	1.62×10^{-2}

The higher frequency of dislocation motions at elevated temperatures gives us more opportunity to study the detailed structural change of a dislocation in a migration process. We found that in the majority of cases the dislocation migration at elevated temperatures is still accomplished by basic glide and climb steps. However, in rare cases, the 5−7 dislocation reconfigures into a complex defect structure as an intermediate state during the migration process. A basic glide step is normally done by a SW bond rotation of two neighboring carbon atoms in the heptagon. However, at 500 °C, we observed a complex glide step in which the two carbon atoms next to the dislocation core (highlighted in red in Figure 6d) underwent a SW rotation in the first place, forming a 555−777 defect structure (Figure 6e), which is reported to have a lower formation energy in carbon nanotubes.[44] The defect can be regarded as the assembly of 5−7 dislocation and a SW defect, or three adjacent dislocation cores. With the SW defect on the left side unwound, the dislocation shifted two lattices away from its original position. The same process has been reported by Lehtinen *et al.* in the TEM imaging of graphene at room temperature using a higher beam current density of 1×10^8 e s^{-1} nm^{-2}.[17]

The climb process could occur in a similar way at 700 °C by generating a complex defect as an intermediated structure. In Figure 7, a SW rotation next to the dislocation core first took place (Figure 7d), forming a defect structure (Figure 7e) which could be seen as the assembly of a 5−7 dislocation and an inversed-Stone−Wales (ISW) defect (the 7557 structure in the dashed ellipse). After the removal of the highlighted carbon dimer in Figure 7e, the defect eventually

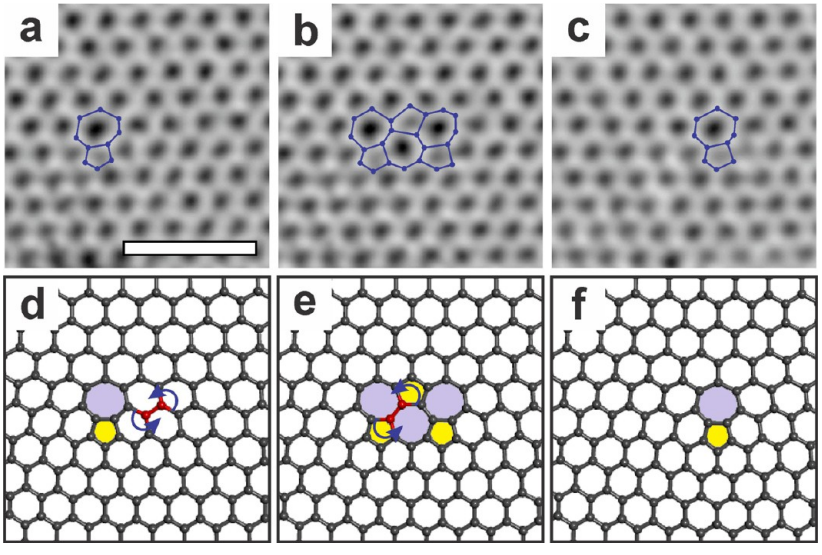

Figure 6. Complex glide of a dislocation in graphene at 500 °C. (a) AC-TEM image of a pentagon−heptagon configured dislocation core. (b) A SW rotation next to the dislocation leads to the formation of three adjacent dislocation cores. (c) The SW defect on the left side is relaxed, leaving a dislocation two lattice away from its original place. (d−f) Atomic models corresponding to the TEM images. The scale bar in panel a is 1 nm. The color scheme in the atomic models represents the number of carbon atoms in each ring, with 5 = yellow and 7 = blue.

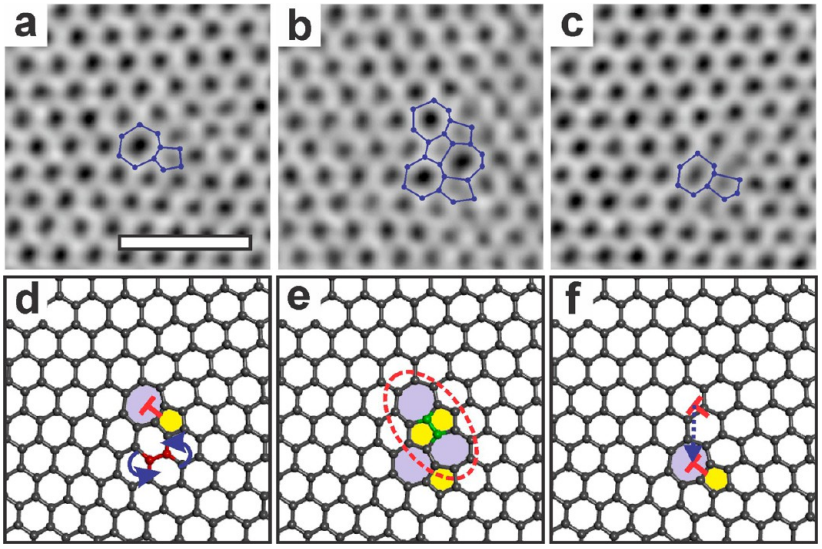

Figure 7. Complex migration of a dislocation at 700 °C. (a) Gaussian-filtered AC-TEM image of a 5−7 dislocation. (b) An evolved dislocation structure following a SW rotation. (c) The removal of a carbon dimer transforms the structure back to a 5−7 dislocation. (d−f) Atomic models corresponding to panel a−c. Bonds that undergo a SW rotation in the next panel are highlighted in red and by the blue arrows. Atoms to be removed are highlighted in green. The scale bar in panel a is 1 nm. The color scheme in the atomic models represents the number of carbon atoms in each ring, with 5 = yellow and 7 = blue.

annealed back to a normal dislocation core, as shown in Figure 7c,f. The whole process is equivalent to one basic glide plus one basic climb step.

We calculated the energy barrier for this process using DFT. The result is shown by the blue curve in Figure 8, with two different possible pathways as a comparison. We find that a bond rotation next to the dislocation core needs to overcome an energy barrier 1.27 eV higher than the bond rotation associated with a basic glide step. On the other hand, the energy barrier for evaporation of the highlighted dimer in the 7557−57 defect in Figure 6e is 1.12 eV lower than a basic climb motion. This is in accordance with our previous work which reported the instability and a relatively short lifetime of a ISW defect under electron irradiation.[45] The total formation energy of the system does not change much after the bond rotation but is increased by 12−13 eV after the dimer sputtering, which explains why the bond rotation is more frequently observed in our experiment than atom displacement.

Figures 9 and 10 are two examples showing more complex evolution of dislocations under electron irradiation at 700 °C. A dislocation core in Figure 9a first underwent carbon dimer sputtering in the pentagon, leading to the formation of a 5−77−5 defect (Figure 9b). A further SW rotation transformed the structure into an irregular configuration consisting of three pentagons and three heptagons as is shown in Figure 9c. The defect subsequently relaxed to the 5−7 configuration and migrated to its position in Figure 9d. A probable order of four SW rotations for this transformation is illustrated schematically by the atomic models in Figure 9g−j.

In Figure 10, we observed one climb step accomplished by the successive sputtering of two nonadjacent carbon atoms. The migration process started from the formation of a 5−8−5 divacancy next to the dislocation (Figure 10a). The defect then evolved into a metastable configuration with bridging atoms (Figure 10c), following the sputtering of one single carbon atom highlighted in green in Figure 10h. It has been previously proposed that under-coordinated carbon atoms in bridging positions play a role in stabilizing odd numbered vacancies under electron irradiation.[30] After the removal of a further atom in Figure 10i, the defect reconfigured into the same structure in Figure 10h. The atomic models in Figure 10h−j can also be regarded as a climb step for the 7−55−8−5 configured dislocation. Afterward, the dislocation transformed to a 5−77−5 structure (Figure 10e) before finally quenched to the 5−7 configuration (Figure 10f). We find that the reconfiguration between Figure 10d and Figure 10e cannot be achieved by merely SW rotations. Figure 10j−m suggests a possible pathway, in which bonds with red crosses in Figure 10j broke initially, followed by the rotation of the red bonds (Figure 10k) and their rebonding with the under-coordinated carbon atoms.

Apart from the step by step random walk, we also observed large-scale jumps of a dislocation between sequential frames. Figure 11a shows a large jump of a dislocation at 500 °C, over a distance of 2.9 nm. The mechanisms for the large jump are likely to be different from the theories we discussed above, as the migration rate is at least 100 times higher. The migration distance is equivalent to 12 basic glide steps, requiring an activation energy of about 84 eV, which is

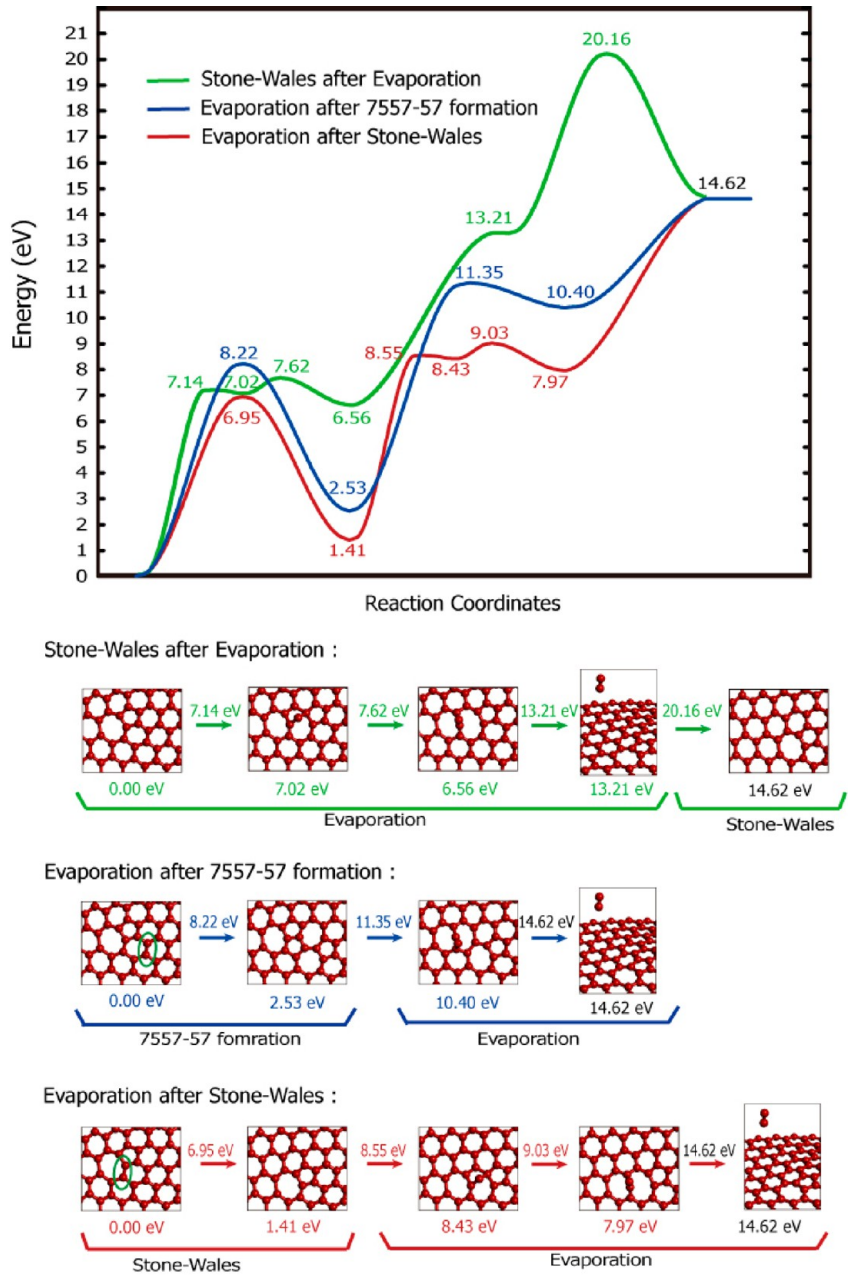

Figure 8. Density functional theory (DFT) simulations showing the energy barrier of different pathways for the structural change in Figure 7. The green curve indicates the pathway in which a SW rotation in the heptagon occurs before the evaporation of a carbon dimer and the red curve otherwise. The mechanism observed in Figure 7 is indicated by the blue curved line.

far more than the maximum energy that one 80 keV electron can impart in a collision at 500 °C (18.6 eV, see Figure S6). It is also worth noting that the glide direction for the dislocation in Figure 3 is randomly distributed, while the large motion consists a dozen of glide steps toward the same direction. Thus, this large glide movement is more likely driven by changes in the local strain at elevated temperatures, such as warping of the sheet or long-range buckling as previously reported.[16] Further work is still required to gain a deeper understanding of this phenomenon. Figure 11c–f gives two more cases at 800 °C, indicating the long-distance glide at 500 °C is not an isolated event.

CONCLUSION

We have used an *in situ* heating holder within an AC-TEM at 80 kV to investigate the atomic-scale motion and configuration of dislocations in graphene as a function of temperature. An increase in the specimen temperature accelerates both glide and climb motions, revealing for the first time temperature driven dynamics of dislocation cores at the atomic level. Instead of the basic glide and climb processes, the dislocation

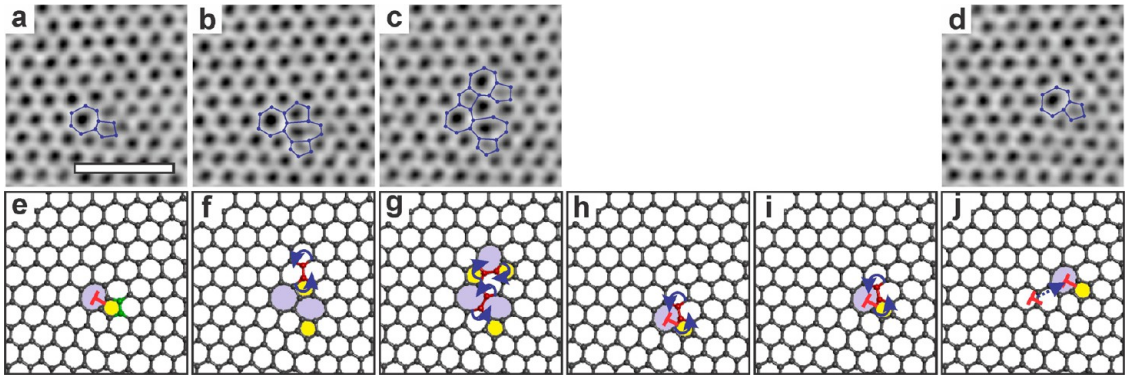

Figure 9. Another example showing a complex migration process at 700 °C. (a) Filtered AC-TEM image of a dislocation core. (b) A 5−77−5 defect after the sputtering of two atoms in the pentagon. (c) An irregular defect structure after two SW rotations, before annealing to the 5−7 dislocation in (d) *via* a few more rotations. (e−g, j) Atomic models for the corresponding TEM images. (g−j) A probable path way for the detailed structure reconfiguration between the defects in panel c and d. The scale bar in panel a is 1 nm.

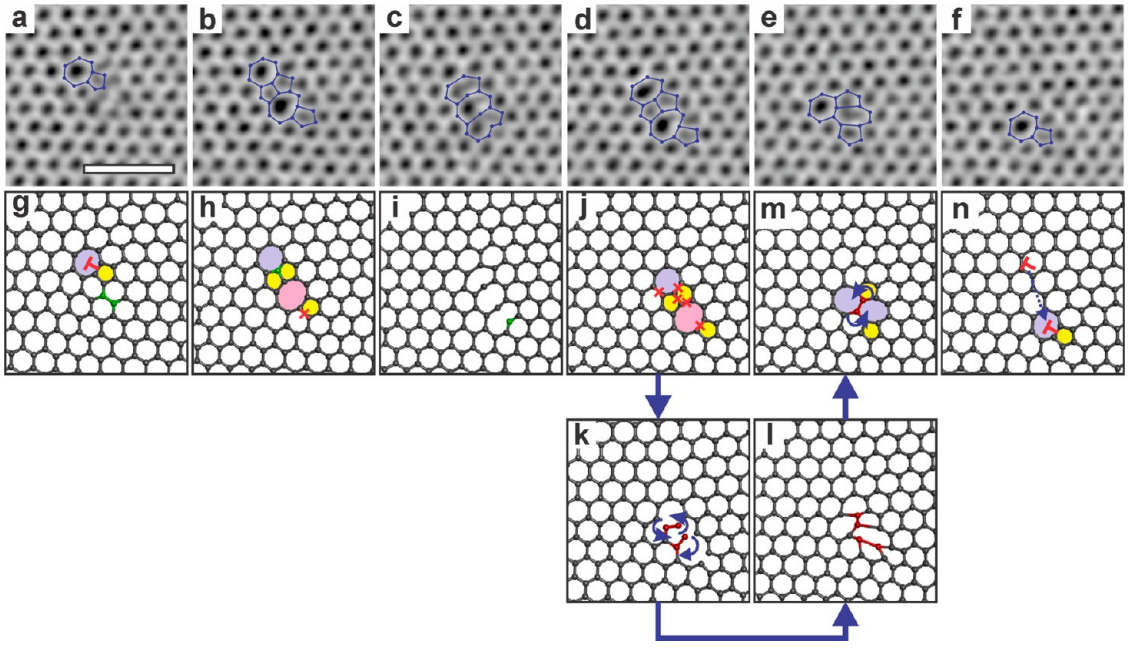

Figure 10. Complex migration of a dislocation at 700 °C *via* the formation of an intermediate structure with bridging atoms. (a) AC-TEM image showing an isolated dislocation core. (b) A 5−8−5 divacancy formed next to the dislocation. (c) The removal of a carbon atom leads to the formation of a defect with bridging atoms. (d) A further atoms is sputtered, yielding to the same defect in panel b. (e) A 5−77−5 defect formed after breakage and rotation of bonds. (f) A finally quenched dislocation core. (g−j, m, n) Atomic models corresponding to the TEM images. (j−m) A possible pathway for the structural change between panels d and e. The scale bar in panel a is 1 nm.

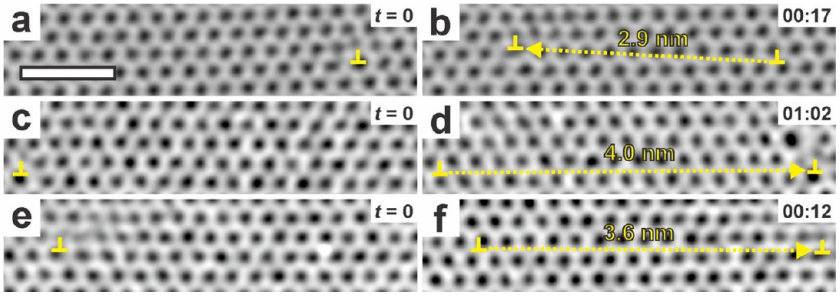

Figure 11. AC-TEM images showing the long-distance glide steps of a dislocation. (a and b) Two consecutive frames taken at 500 °C with a time interval of 17 s, showing a large glide motion of a dislocation core over 2.9 nm. (c−f) Two more examples of the large glide motions taken at 800 °C, where the time interval is 62 and 12 s and jump distance is 4.0 and 3.6 nm, respectively. The scale bar in panel a is 1 nm.

migration sometimes takes the form of a complex defect as a metastable structure. The instantaneous slip of a dislocation over more than 10 lattices in the heated graphene shows substantial dynamics are occurring in the system that might be active by applying stress fields to change the strain. By presenting the detailed study on high temperature stability of dislocations in graphene, we hope to provide insights into future studies in defect-related nanoengineering and property modification in graphene.

METHODS

Synthesis of Graphene. Monolayer graphene was synthesized by atmospheric pressure chemical vapor deposition (CVD) method using a melted copper sheet as the catalyst as previously reported.[46] The high purity copper foil (Alfa Aesar, Puratonic 99.999% pure, 0.1 mm thick) of ~1 cm^2 was placed on a molybdenum piece of the same size (Alfa Aesar, 99.95% pure, 0.1 mm thick), which were both loaded into a 1 in. quartz tube in the CVD system. Molybdenum acts as a stable wetting layer to prevent liquid copper from balling. Then, 100 sccm H_2/Ar (20% H_2 in Ar), 100sccm CH_4 (1% CH_4 in Ar) and 200 sccm 100% Ar were flowed for 30 min. CH_4 flow was switched off before increasing the hot-zone temperature to 1090 °C. Once the temperature reached 1090 °C, the quartz tube was moved from the room temperature zone to the center of heating zone and the mixture annealed for 30 min. The flow of H_2/Ar was then reduced to 80 sccm, and 10 sccm of 1% CH_4 in Ar was added for 90 min for graphene growth. After growth, the quartz was removed from the heating zone for rapid cooling in the air with CH_4 off.

Transfer. A PMMA scaffold (8 wt % in anisole, 495K molecular weight) was spin-coated onto the graphene sheet at 4700 rpm for 60 s and then baked at 180 °C for 90 s to solidify. Afterward, the sample was made up of a molybdenum/copper/graphene/PMMA stack. The copper layer was etched by floating the sample on the mixed solution of iron(III) chloride and hydrochloride, leaving a floating graphene−PMMA film on the top after 48 h. The film was collected using a clean glass slide and transferred onto the surface of the DI water for 30 min to wash away the remaining iron(III) chloride. To further dissolve excess iron chloride, the sample was transferred onto a 10% hydrogen chloride solution for 5 min, before it was rinsed again in the DI water for 30 min. The film was then transferred onto a SiN TEM grid designed for *in situ* Transmission Electron Microscopy in a heating holder (DENSsolutions single tilt 30° fitted with DENSsolutions High Temperature EM heater chip with a maximum operating temperature up to 800 °C). The thin SiN membrane on the heating holder contained several windows (size 3 × 0.2 μm) produced using a Zeiss NVision SEM: FIB prior to graphene transfer. These windows were essential to enable HRTEM imaging of the graphene lattice without contrast from the SiN membrane. The grid was then cured at 350 °C for 12 h to burn out PMMA, leaving only graphene layer on it.

Electron Microscopy. HRTEM images were taken at an accelerating voltage of 80 kV, using Oxford's JEOL JEM-2200MCO field emission transmission electron microscope with a CEOS image corrector.[16] Dislocations were introduced using a focused electron beam according to our previously reported procedure.[37] Data were recorded using a Gatan Ultrascan 4K × 4K CCD camera with 1−4 s acquisition times. TEM images were processed using ImageJ. Smoothing of images was achieved by using a Gaussian blur filter in ImageJ.

Heating Holder. To perform variable-temperature experiments, we used a commercially available *in situ* heating holder from DENS Solutions (SH30-4M-FS). In the DENS Solutions holder, heating of the sample was achieved by passing a current through a platinum resistive coil imbedded in the TEM chip (DENS Solutions DENS-C-30). The resistance of the platinum coil is monitored in a four-point configuration, and the temperature is calculated using the Callendar−Van Dusen equation (with calibration constants provided by the manufacturer).

Density Functional Theory (DFT) Calculation. The DFT calculations were performed within the generalized gradient approximation (GGA) of Perdew−Burke−Ernzerhof (PBE) functional using the Vienna *ab initio* simulation package (VASP) code. The unit cells were constructed by removing 16 carbon atoms to make two dislocation cores from a pristine graphene structure of 480 carbon atoms. We also included a vacuum region of 30 Å in the *z* direction of the supercell. The Brillouin zone was sampled using a (1 × 2 × 1) Γ centered mesh. The energy cutoff for plane wave basis set was 400 eV. When structural relaxations were performed, the structure was fully relaxed until the force on each atom was smaller than 0.02 eV/Å.

Conflict of Interest: The authors declare no competing financial interest.

Acknowledgment. J.H.W. thanks the support from the Royal Society. C.G. thanks the support from the Clarendon Fund. G.-D. L. and E.Y. acknowledge support from the Supercomputing Center/Korea Institute of Science and Technology Information with supercomputing resources (KSC-2014-C3-009), from the BK21 plus program, and from the National Research Foundation of Korea (NRF) grant funded by the Korea government (RIAM No. 2010-0012670). C.S.A. acknowledges support from the ESTEEM2 (Enabling Science and Technology through European Electron Microscopy) project (7th Framework Programme of the European Commission).

Supporting Information Available: The Supporting Information is available free of charge on the ACS Publications website at DOI: 10.1021/acsnano.5b05355.

Other examples of dislocation migration at 500 and 700 °C, plots showing the distribution of the number of scattering events per second with transferred energy, the temperature dependence of average kinetic energy of carbon atoms and the maximum transferred energy at 80 kV and TEM images (PDF)

REFERENCES AND NOTES

1. Novoselov, K. S.; Geim, A. K.; Morozov, S. V.; Jiang, D.; Zhang, Y.; Dubonos, S. V.; Grigorieva, I. V.; Firsov, A. A. Electric Field Effect in Atomically Thin Carbon Films. *Science* **2004**, *306*, 666–669.
2. Castro Neto, A. H.; Peres, N. M. R.; Novoselov, K. S.; Geim, A. K. The Electronic Properties of Graphene. *Rev. Mod. Phys.* **2009**, *81*, 109–162.
3. Bae, S.; Kim, H.; Lee, Y.; Xu, X.; Park, J.-S.; Zheng, Y.; Balakrishnan, J.; Lei, T.; Kim, H. R.; Song, Y. Il; et al. Roll-to-Roll Production of 30-Inch Graphene Films for Transparent Electrodes. *Nat. Nanotechnol.* **2010**, *5*, 574–578.
4. Lee, C.; Wei, X.; Kysar, J. W.; Hone, J. Measurement of the Elastic Properties and Intrinsic Strength of Monolayer Graphene. *Science* **2008**, *321*, 385–388.
5. Faccio, R.; Mombrú, A. W. Magnetism in Multivacancy Graphene Systems. *J. Phys.: Condens. Matter* **2012**, *24*, 375304.
6. Krasheninnikov, A. V.; Lehtinen, P. O.; Foster, A. S.; Pyykkö, P.; Nieminen, R. M. Embedding Transition-Metal Atoms in Graphene: Structure, Bonding, and Magnetism. *Phys. Rev. Lett.* **2009**, *102*, 126807.
7. He, Z.; He, K.; Robertson, A. W.; Kirkland, A. I.; Kim, D.; Ihm, J.; Yoon, E.; Lee, G.-D.; Warner, J. H. Atomic Structure and Dynamics of Metal Dopant Pairs in Graphene. *Nano Lett.* **2014**, *14*, 3766–3772.
8. Santos, E. J. G.; Ayuela, A.; Sánchez-Portal, D. First-Principles Study of Substitutional Metal Impurities in Graphene: Structural, Electronic and Magnetic Properties. *New J. Phys.* **2010**, *12*, 053012.

9. Yazyev, O. Magnetism in Disordered Graphene and Irradiated Graphite. *Phys. Rev. Lett.* **2008**, *101*, 037203.
10. Jeong, B.; Ihm, J.; Lee, G.-D. Stability of Dislocation Defect with Two Pentagon-Heptagon Pairs in Graphene. *Phys. Rev. B: Condens. Matter Mater. Phys.* **2008**, *78*, 165403.
11. Lee, G.-D.; Yoon, E.; Hwang, N.-M.; Wang, C.-Z.; Ho, K.-M. Formation and Development of Dislocation in Graphene. *Appl. Phys. Lett.* **2013**, *102*, 021603.
12. Yakobson, B. I. Mechanical Relaxation and "intramolecular Plasticity" in Carbon Nanotubes. *Appl. Phys. Lett.* **1998**, *72*, 918–920.
13. Ding, F.; Jiao, K.; Wu, M.; Yakobson, B. I. Pseudoclimb and Dislocation Dynamics in Superplastic Nanotubes. *Phys. Rev. Lett.* **2007**, *98*, 75503.
14. Ding, F.; Jiao, K.; Lin, Y.; Yakobson, B. I. How Evaporating Carbon Nanotubes Retain Their Perfection? *Nano Lett.* **2007**, *7*, 681–684.
15. Yazyev, O. V.; Louie, S. G. Topological Defects in Graphene: Dislocations and Grain Boundaries. *Phys. Rev. B: Condens. Matter Mater. Phys.* **2010**, *81*, 195420.
16. Warner, J. H.; Margine, E. R.; Mukai, M.; Robertson, A. W.; Giustino, F.; Kirkland, A. I. Dislocation-Driven Deformations in Graphene. *Science* **2012**, *337*, 209–212.
17. Lehtinen, O.; Kurasch, S.; Krasheninnikov, a V; Kaiser, U. Atomic Scale Study of the Life Cycle of a Dislocation in Graphene from Birth to Annihilation. *Nat. Commun.* **2013**, *4*, 2098.
18. Meyer, J. C.; Geim, A. K.; Katsnelson, M. I.; Novoselov, K. S.; Booth, T. J.; Roth, S. The Structure of Suspended Graphene Sheets. *Nature* **2007**, *446*, 60–63.
19. Fasolino, A.; Los, J. H.; Katsnelson, M. I. Intrinsic Ripples in Graphene. *Nat. Mater.* **2007**, *6*, 858–861.
20. Warner, J. H.; Fan, Y.; Robertson, A. W.; He, K.; Yoon, E.; Lee, G.-D. Rippling Graphene at the Nanoscale through Dislocation Addition. *Nano Lett.* **2013**, *13*, 4937–4944.
21. Gong, C.; He, K.; Robertson, A. W.; Yoon, E.; Lee, G.-D.; Warner, J. H. Spatially Dependent Lattice Deformations for Dislocations at the Edges of Graphene. *ACS Nano* **2015**, *9*, 656–662.
22. Lee, G.-D.; Yoon, E.; He, K.; Robertson, A. W.; Warner, J. H. Detailed Formation Processes of Stable Dislocations in Graphene. *Nanoscale* **2014**, *6*, 14836–14844.
23. Kotakoski, J.; Mangler, C.; Meyer, J. C. Imaging Atomic-Level Random Walk of a Point Defect in Graphene. *Nat. Commun.* **2014**, *5*, 3991.
24. Suenaga, K.; Wakabayashi, H.; Koshino, M.; Sato, Y.; Urita, K.; Iijima, S. Imaging Active Topological Defects in Carbon Nanotubes. *Nat. Nanotechnol.* **2007**, *2*, 358–360.
25. He, K.; Robertson, A. W.; Fan, Y.; Allen, C. S.; Lin, Y.-C.; Suenaga, K.; Kirkland, A. I.; Warner, J. H. Temperature Dependence of the Reconstruction of Zigzag Edges in Graphene. *ACS Nano* **2015**, *9*, 4786.
26. Huang, J. Y.; Chen, S.; Wang, Z. Q.; Kempa, K.; Wang, Y. M.; Jo, S. H.; Chen, G.; Dresselhaus, M. S.; Ren, Z. F. Superplastic Carbon Nanotubes. *Nature* **2006**, *439*, 281.
27. Huang, J. Y.; Ding, F.; Jiao, K.; Yakobson, B. I. Real Time Microscopy, Kinetics, and Mechanism of Giant Fullerene Evaporation. *Phys. Rev. Lett.* **2007**, *99*, 175503.
28. Hawkes, P. W. Aberration Correction Past and Present. *Philos. Trans. R. Soc., A* **2009**, *367*, 3637–3664.
29. Robertson, A. W.; Warner, J. H. Atomic Resolution Imaging of Graphene by Transmission Electron Microscopy. *Nanoscale* **2013**, *5*, 4079–4093.
30. Robertson, A. W.; Lee, G.-D.; He, K.; Yoon, E.; Kirkland, A. I.; Warner, J. H. The Role of the Bridging Atom in Stabilizing Odd Numbered Graphene Vacancies. *Nano Lett.* **2014**, *14*, 3972–3980.
31. Robertson, A. W.; Lee, G.-D.; He, K.; Yoon, E.; Kirkland, A. I.; Warner, J. H. Stability and Dynamics of the Tetravacancy in Graphene. *Nano Lett.* **2014**, *14*, 1634–1642.
32. Gong, C.; Robertson, A. W.; He, K.; Ford, C.; Watt, A. a R.; Warner, J. H. Interactions of Pb and Te Atoms with Graphene. *Dalton Trans.* **2014**, *43*, 7442–7448.
33. Zobelli, A.; Gloter, A.; Ewels, C. P.; Seifert, G.; Colliex, C. Electron Knock-on Cross Section of Carbon and Boron Nitride Nanotubes. *Phys. Rev. B: Condens. Matter Mater. Phys.* **2007**, *75*, 245402.
34. Warner, J. H.; Rümmeli, M. H.; Ge, L.; Gemming, T.; Montanari, B.; Harrison, N. M.; Büchner, B.; Briggs, G. A. D. Structural Transformations in Graphene Studied with High Spatial and Temporal Resolution. *Nat. Nanotechnol.* **2009**, *4*, 500–504.
35. Meyer, J. C.; Kisielowski, C.; Erni, R.; Rossell, M. D.; Crommie, M. F.; Zettl, A. Direct Imaging of Lattice Atoms and Topological Defects in Graphene Membranes. *Nano Lett.* **2008**, *8*, 3582–3586.
36. Meyer, J. C.; Eder, F.; Kurasch, S.; Skakalova, V.; Kotakoski, J.; Park, H. J.; Roth, S.; Chuvilin, A.; Eyhusen, S.; Benner, G. Accurate Measurement of Electron Beam Induced Displacement Cross Sections for Single-Layer Graphene. *Phys. Rev. Lett.* **2012**, *108*, 196102.
37. Robertson, A. W.; Allen, C. S.; Wu, Y. A.; He, K.; Olivier, J.; Neethling, J.; Kirkland, A. I.; Warner, J. H. Spatial Control of Defect Creation in Graphene at the Nanoscale. *Nat. Commun.* **2012**, *3*, 1144.
38. Li, L.; Reich, S.; Robertson, J. Defect Energies of Graphite: Density-Functional Calculations. *Phys. Rev. B: Condens. Matter Mater. Phys.* **2005**, *72*, 184109.
39. Kim, Y.; Ihm, J.; Yoon, E.; Lee, G.-D. Dynamics and Stability of Divacancy Defects in Graphene. *Phys. Rev. B: Condens. Matter Mater. Phys.* **2011**, *84*, 075445.
40. Kotakoski, J.; Meyer, J. C.; Kurasch, S.; Santos-Cottin, D.; Kaiser, U.; Krasheninnikov, a. V. Stone-Wales-Type Transformations in Carbon Nanostructures Driven by Electron Irradiation. *Phys. Rev. B: Condens. Matter Mater. Phys.* **2011**, *83*, 245420.
41. Wang, Z.; Zhou, Y. G.; Bang, J.; Prange, M. P.; Zhang, S. B.; Gao, F. Modification of Defect Structures in Graphene by Electron Irradiation: Ab Initio Molecular Dynamics Simulations. *J. Phys. Chem. C* **2012**, *116*, 16070–16079.
42. Krasheninnikov, A. V.; Banhart, F.; Li, J. X.; Foster, A. S.; Nieminen, R. M. Stability of Carbon Nanotubes under Electron Irradiation: Role of Tube Diameter and Chirality. *Phys. Rev. B: Condens. Matter Mater. Phys.* **2005**, *72*, 125428.
43. Lehtinen, O.; Kotakoski, J.; Krasheninnikov, A. V.; Tolvanen, A.; Nordlund, K.; Keinonen, J. Effects of Ion Bombardment on a Two-Dimensional Target: Atomistic Simulations of Graphene Irradiation. *Phys. Rev. B: Condens. Matter Mater. Phys.* **2010**, *81*, 153401.
44. Chen, S.; Ertekin, E.; Chrzan, D. C. Plasticity in Carbon Nanotubes: Cooperative Conservative Dislocation Motion. *Phys. Rev. B: Condens. Matter Mater. Phys.* **2010**, *81*, 155417.
45. Robertson, A. W.; He, K.; Kirkland, A. I.; Warner, J. H. Inflating Graphene with Atomic Scale Blisters. *Nano Lett.* **2014**, *14*, 908–914.
46. Fan, Y.; He, K.; Tan, H.; Speller, S.; Warner, J. H. Crack-Free Growth and Transfer of Continuous Monolayer Graphene Grown on Melted Copper. *Chem. Mater.* **2014**, *26*, 4984–4991.